 doi: 10.1111/j.1365-246X.2007.03391.x

Evolution of stress in Southern California for the past 200 years from coseismic, postseismic and interseismic stress changes

Andrew M. Freed,[1] Syed Tabrez Ali[1] and Roland Bürgmann[2]

[1]*Department of Earth and Atmospheric Sciences, Purdue University,* 550 *Stadium Mall Dr., West Lafayette,* IN 47907*, USA. E-mail: freed@purdue.edu*
[2]*Department of Earth and Planetary Science,* 389 *McCone Hall, University of California, Berkeley, Berkeley,* CA 94720*, USA*

Accepted 2007 January 11. Received 2007 January 11; in original form 2006 April 13

SUMMARY

The seismicity of southern California results from stresses that arise from the relative motion of the Pacific and North American Plates being accommodated along the San Andreas Fault (SAF) system and the Eastern California Shear Zone (ECSZ). Here we calculate how the stress field in southern California has evolved over the past two centuries due to interseismic loading, as inferred from current GPS observations of surface velocities, from redistributions of static stress induced by large ($M_w \geq 6.5$) earthquakes since the 1812 Wrightwood quake, and postseismic viscoelastic relaxation associated with these events that serves to transfer coseismic stresses from the deep, warm, lower crust and upper mantle to the overlying seismogenic upper crust. We calculate Coulomb stress changes on vertical strike-slip faults striking parallel to the SAF and at the hypocenters on the rupture planes of all $M_w \geq 6$ events over the past two centuries. Our results suggest that the 1857 $M_w = 8.2$ Fort Tejon earthquake, by far the largest event to have occurred in the region over the past two centuries, had a profound influence on the state of stress in Southern California during the 19th century, inducing significant stress increases to the north (Parkfield region and adjoining creeping SAF) and south (southern SAF and San Jacinto fault), and stress relief across the southern ECSZ. These stress changes were then greatly magnified by postseismic relaxation through the early part of the 20th century. Slow interseismic build-up of stress further loads all major strike-slip faults and works to reload the areas of the ECSZ where stress was relieved by the 1857 quake. Our calculations suggest that only 56% of hypocenters were pushed closer to failure by preceding coseismic stress changes, suggesting that the occurrence of large earthquakes is not strongly determined by coseismic Coulomb stress changes. This percentage rises to 70% when postseismic stress changes are also considered. Our calculations demonstrate the importance of postseismic viscoelastic relaxation in the redistribution of stress following large earthquakes. We find, however, that postseismic processes associated with events more than about a decade old are near completion and thus do not significantly influence the regional velocity field presently observed in southern California.

Key words: California, Coulomb, earthquake, triggering, viscoelastic.

1 INTRODUCTION

Having experienced more than 73 $M_w \geq 6$ earthquakes since 1812 (Kagan *et al.* 2006) (Fig. 1), southern California is one of the most seismically active regions in the conterminous United States. This high seismicity rate is a product of ~50 mm yr^{-1} of relative motion between the North American and Pacific plates (DeMets & Dixon 1999), accommodated primarily by right-lateral slip on the San Andreas Fault (SAF), other subparallel faults and the Eastern California Shear zone (ECSZ). The southern SAF is capable of producing major ($M_w > 7.5$) earthquakes, two of which have occurred in the past 200 yr; at Wrightwood in 1812 ($M_w = 7.5$) and Fort Tejon in 1857 ($M_w = 8.2$) (Jacoby *et al.* 1988; Sieh *et al.* 1989); and the recent 1992 $M_w = 7.3$ Landers and 1999 $M_w = 7.1$ Hector Mine earthquakes showed that the ECSZ is also capable of producing large events. In addition, the bend in the SAF in southern California has led to a zone of compression forming the Transverse Ranges and thrust earthquakes in the Los Angeles region, such as the 1994 $M_w = 6.7$ Northridge earthquake.

Numerous studies have sought to understand the distribution of large earthquakes in space and time in southern California with the hope of improving forecasting and mitigation. Many of these efforts have concentrated on calculating the evolution of crustal stresses as a means to understanding patterns of earthquake occurrence. In a process referred to as fault interaction, earthquakes have been theorized to encourage or retard subsequent earthquakes in a region (see reviews by Harris 1998; Stein 1999, 2003; King & Cocco 2001; Freed 2005). In some regions large earthquakes appear to be explained

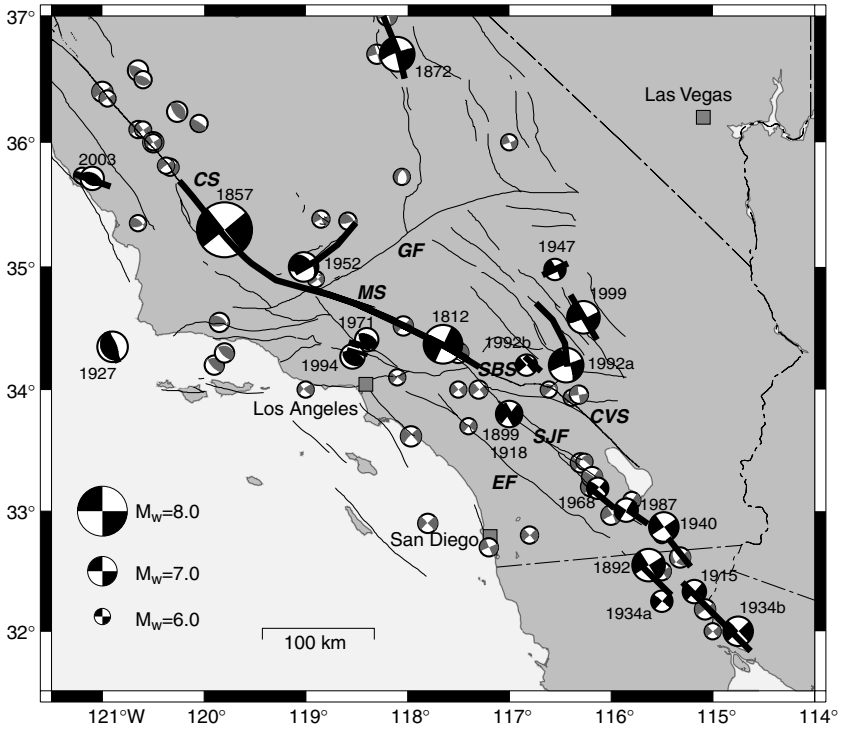

Figure 1. Earthquakes in southern California between 1812 and 2005 considered in this analysis. Black and white focal mechanisms show 21 earthquakes of $M_w \geq 6.5$ that are used to determine how coseismic slip and associated postseismic relaxation has influenced the southern California stress field since 1812 (Table 1). Grey and white focal mechanisms show 52 $6.0 \leq M_w < 6.5$ events where stress changes are determined for each hypocenter prior to rupture, but stress changes due to these ruptures are not considered (Table 2). Earthquake dates are only shown for $M_w \geq 6.5$ events. Thick lines show approximate rupture surface trace (or projected surface trace for blind thrusts) associated with each $M_w \geq 6.5$ event. Segments of the San Andreas Fault: CS—Cholame segment, MS—Mojave segment, SBS—San Bernardino Mountain segment, CVS—Coachella Valley segment, SJF—San Jacinto Fault, EF—Elsinore Fault.

simply by knowing how stress has evolved over the past century or two based on stress changes associated with earthquake slip and interseismic loading. No knowledge of the stress field prior to the relatively short study period appears to be required. Studies of changes in Coulomb stress, which considers both shear- and normal-stress changes to quantify whether faults have been pushed closer to (positive Coulomb stress change) or further away from (negative Coulomb stress change) failure by nearby earthquakes, have shown to be particularly revealing (e.g. Jaeger & Cook 1979; Stein & Lisowski 1983; King *et al.* 1994). For example, Stein *et al.* (1994) show that the 1933 $M_w = 6.4$ Long Beach and 1952 $M_w = 7.3$ Kern County, California earthquakes combined to increase Coulomb stress at the eventual hypocenter of the 1971 $M_w = 6.7$ San Fernando earthquake, which in turn increased Coulomb stress at the eventual hypocenter of the 1994 $M_w = 6.7$ Northridge quake. Coseismic stress changes associated with earthquakes can also unload nearby faults and potentially induce a period of seismic quiescence (e.g. Scholz 1988; Harris & Simpson 1996, 1998). For example, the 1906 San Francisco earthquake initiated a period of seismic quiescence in the Bay area in which only 2 $M_w \geq 6$ earthquakes occurred in the 75 yr following the great quake compared to 15 in the 75 yr prior (Bakun 1999).

Fault interaction is, however, most likely a much more complicated process than the simple relationships inferred from coseismic (static) stress changes and seismicity in some studies. First, several statistical studies suggest that stress shadows, regions in which seismicity appears to be reduced by a drop in Coulomb stress due to a nearby earthquake (e.g. Harris & Simpson 1996), do not appear to exist for some events (e.g. Felzer & Brodsky 2005). Secondly, factors other than static stress changes may be as or much more important to the triggering process. Several studies suggest that the rate at which static stress changes occur may be more important than the magnitude (e.g. Toda & Stein 2003; Toda *et al.* 2005). In this scenario, even small coseismic stress changes may be more important than larger postseismic or interseismic stress changes because they are sudden, causing a much higher rate of triggered seismicity which then decays inversely with time. Another possibility, known as dynamic triggering, is that the passage of transient seismic waves induce significant, but temporary, stress changes which trigger seismicity both close to the rupture and as far as thousands of kilometres away (e.g. Gomberg 1996; Kilb *et al.* 2000; Gomberg *et al.* 2004). Several studies suggest that dynamic triggering may be significantly more influential on the triggering of aftershocks than static stress changes (e.g. Felzer & Brodsky 2006), though the process by which transient seismic waves can induce longer-term (beyond a few days) triggering is not clear. In the present study we calculate how static stress changes evolved at the hypocenter of historic earthquakes in southern California due to coseismic, postseismic and interseismic mechanisms to illuminate how such stress changes relate to earthquake occurrence. We do not attempt to prove that coseismic and postseismic stress changes are in fact responsible for earthquake triggering.

Deng & Sykes (1997a,b) explored the relationship between seismicity and Coulomb stress changes in southern California over the past two centuries by considering not only sudden stress changes due to all major earthquakes, but also due to the steady, long-term

accumulation of stress resulting from the relative motion of the North American and Pacific plates. They found that 95% of 37 M ≥ 6 earthquakes that occurred in southern California between 1812 and 1995 and 85% of 138 M ≥ 5 earthquakes from 1932 to 1995, occurred on faults with Coulomb stress increases from major earthquakes and interseismic loading since 1812. This study did not, however, take into account the process of postseismic relaxation of a viscous lower crust and upper mantle which, following major earthquakes, can transfer significant stress upwards to the seismogenic shallow crust (e.g. Pollitz 1995; Freed & Lin 1998; Chéry *et al.* 2001; Marsan & Bean 2003). A number of studies have shown that such stress transfer can have a broad impact on the evolution of the stress field (e.g. Freed & Lin 2002; Pollitz *et al.* 2003; Smith & Sandwell 2006). In southern California, stress increases at the eventual hypocenter of the 1999 Hector Mine earthquake induced by viscoelastic relaxation following the nearby 1992 Landers quake, may have influenced the 7-yr time interval between the Landers and the subsequent Hector Mine earthquake (Freed & Lin 2001; Zeng 2001; Pollitz & Sacks 2002). Freed & Lin (2002) showed that the combined influence of viscous relaxation following the Landers and Hector Mine earthquakes has induced (and is continuing to induce) a migration of stress westwards towards the San Andreas, San Jacinto and Elsinore faults, bringing these faults closer to failure.

Previous models of interseismic loading in southern California assumed that interseismic strain is associated with deep slip on the major faults below an inferred locking depth (e.g. Deng & Sykes 1997a,b; Smith & Sandwell 2003, 2006; Meade & Hager 2005). Parsons (2002, 2006), however, showed that interseismic stressing rates may be much lower than those predicted by deep slip models if deformation at depth is distributed within a viscoelastic lower crust and mantle. As an alternative, Pollitz & Nyst (2005) considered interseismic deformation in the San Francisco Bay region to be accommodated across a broad shear zone representative of regional weakness due to the presence of a thinner lithosphere. In addition, several studies suggest that repeated postseismic relaxation processes through multiple earthquake cycles could lead to a build-up of a steady-state background strain rate that could influence interseismic loading (Savage & Lisowski 1998; Segall 2002; Dixon *et al.* 2003; Johnson & Segall 2004; ; Hetland & Hager 2005; Kenner & Simons 2005).

Here we expand on the calculations by Deng & Sykes (1997a, b) by considering stress transfer due to postseismic relaxation and by calculating interseismic stress rates from strain rates calculated directly from surface velocities from the Southern California Earthquake Center (SCEC) Crustal Motion Map (Version 3) (http://epicenter.usc.edu/cmm3, Shen *et al.* 2003). By calculating stress rates from surface velocities we avoid any assumptions regarding mechanisms of interseismic strain accumulation. The limitation of such an approach is that we assume that accumulating interseismic strains are uniform with depth through the seismogenic upper crust.

The calculations consider how stress in southern California has been modified by 21 $M_w \geq 6.5$ events since 1812 (Table 1, black focal mechanisms in Fig. 1). These represent all large events over the past two centuries in which a reasonable characterization of the slip distribution has been determined. Except were noted in Table 1, we use the same slip distributions as Deng & Sykes (1997a,b). In addition to the $M_w \geq 6.5$ events, we consider how stress changes

Table 1. $M_w \geq 6.5$ earthquakes in southern California over the past two centuries used to calculate changes to the stress field and the stress changes at their respective hypocenters just prior to rupture (see Fig. 1). A (T) after the location name denotes an event which has a significant thrust component, in which case $\mu' = 0.8$ is assumed, otherwise $\mu' = 0.4$ is assumed. Lat./Lon. indicates the latitude and longitude of the hypocenters of these events. Strike/Dip/Rake indicates the sense of slip at the hypocenter. $\Delta\sigma_c$ Co is the change in coseismic Coulomb stress at the hypocenter due to previous earthquakes. $\Delta\sigma_c$ Post. is the change in Coulomb stress due to viscoelastic relaxation associated with previous events. $\Delta\sigma_c$ Inter. is the change in Coulomb stress due to the regional strain rate field from GPS from 1812 to just before rupture. $\Delta\sigma_c$ Net is the sum of coseismic, postseismic, and interseismic Coulomb stress changes from 1812 to just prior to rupture. Reference numbers refer to the source for both hypocenter location and slip distribution: 1. Deng & Sykes 1997a, 2. Deng & Sykes 1997b, 3. Helmberger *et al.* 1992, 4. Hurst *et al.* 2000, 5. Hardebeck *et al.* 2004. Notes: For the 1952 Kern County earthquake we use the hypocenter fault plane orientation from Lin & Stein (2004) and a depth of 20 km. For the 1971 San Fernando earthquake we use the hypocenter fault plane orientation from Heaton (1982). Coseismic stress change due to the 1899 event on the 1918 San Jacinto hypocenter is neglected due to errors caused by overlap of these events

Year	Location	Lat.	Lon.	M_w	Strike/Dip/Rake	Ref.	$\Delta\sigma_c$ Co. (MPa)	$\Delta\sigma_c$ Post. (MPa)	$\Delta\sigma_c$ Inter. (MPa)	$\Delta\sigma_c$ Net (MPa)
1812	Wrightwood	34.37	−117.65	7.50	295/90/180	1	0.000	0.000	0.000	0.000
1857	Fort Tejon	35.30	−119.80	8.20	321/90/180	1	0.033	0.008	0.509	0.550
1872	Owens Valley	36.70	−118.10	7.30	340/80/−171	1	0.004	0.016	0.121	0.141
1892	Laguna Salada	32.55	−115.63	7.20	328/90/180	1	0.017	0.040	0.923	0.979
1899	San Jacinto	33.80	−117.00	6.70	309/90/180	2	0.120	0.167	0.655	0.942
1915	Volcano Lake	32.33	−115.18	6.60	312/88/180	2	−0.562	0.188	1.397	1.023
1918	San Jacinto	33.80	−117.00	6.80	150/87/−176	2	0.368	0.188	0.878	1.434
1927	Lompoc (T)	34.35	−120.90	6.60	340/66/95	3	−0.046	−0.042	0.039	−0.049
1934a	Laguna Salada	32.25	−115.50	6.50	311/88/180	2	0.181	0.436	1.493	2.111
1934b	Co. River Delta	32.00	−114.75	7.00	317/89/180	2	0.133	0.056	1.199	1.388
1940	Imperial Valley	32.87	−115.48	7.00	325/90/180	1	0.122	0.314	2.985	3.421
1947	Manix	34.98	−116.55	6.50	65/85/8	2	−0.040	−0.176	1.245	1.030
1952	Kern County (T)	35.00	−119.02	7.50	51/75/25	1	2.991	−0.304	−0.384	2.303
1968	Borrego Mountain	33.19	−116.13	6.50	311/78/179	2	0.068	0.106	2.143	2.318
1971	San Fernando (T)	34.41	−118.40	6.60	255/53/75	2	1.633	−0.456	−0.320	0.857
1987	Superstition Hills	33.01	−115.85	6.60	303/90/180	2	0.074	0.218	1.378	1.670
1992a	Landers	34.20	−116.44	7.30	340/74/−176	1	−0.164	−0.010	2.514	2.339
1992b	Big Bear	34.20	−116.83	6.50	48/90/0	1	−0.467	0.022	1.925	1.480
1994	Northridge (T)	34.27	−118.54	6.70	128/33/106	1	0.016	−0.018	0.160	0.158
1999	Hector Mine	34.59	−116.27	7.20	336/80/174	4	−0.325	−0.009	1.047	0.713
2003	San Simeon (T)	35.71	−121.10	6.60	296/50/90	5	−0.035	0.053	−0.313	−0.296

Table 2. Coulomb stress changes since 1812 just prior to rupture at the hypocenters of $6.0 \leq M_w < 6.5$ earthquakes in southern California over the past two centuries. A (T) after the location name denotes an event which has a significant thrust component, in which case $\mu' = 0.8$ is assumed, otherwise $\mu' = 0.4$ is assumed. Lat./Lon. indicates the latitude and longitude of the hypocenters of these events. Strike/Dip/Rake indicates the sense of slip at the hypocenter. $\Delta\sigma_c$ Co Lon. is the change in coseismic Coulomb stress at the hypocenter due to previous earthquakes. Dashed values indicate that the hypocenter was too close to a previous rupture to reasonably calculate coseismic stress changes. $\Delta\sigma_c$ Post. is the change in Coulomb stress due to viscoelastic relaxation associated with previous events. $\Delta\sigma_c$ Inter. is the change in Coulomb stress due to the regional strain rate field from GPS from 1812 to just before rupture. $\Delta\sigma_c$ Net is the sum of coseismic, postseismic and interseismic Coulomb stress changes from 1812 to just prior to rupture. Hypocenters locations and sense of slip are from Kagan *et al.* (2006)

Year	Location	Lat.	Lon.	M_w	Strike/Dip/Rake	$\Delta\sigma_c$ Co. (MPa)	$\Delta\sigma_c$ Post. (MPa)	$\Delta\sigma_c$ Inter. (MPa)	$\Delta\sigma_c$ Net (MPa)
1821	Santa Barbara (T)	34.55	119.85W	6.30	306/47/128	−0.038	−0.004	0.017	−0.016
1827	LA Region	34.00	119.00	6.00	136/79/158	−0.033	−0.015	0.028	−0.020
1830	San Luis Obispo	35.35	120.65	6.00	313/56/136	0.003	0.020	0.048	0.071
1853	NW of Parkfield	36.40	121.00	6.40	145/88/180	0.003	0.006	0.135	0.144
1855	LA Region	34.10	118.10	6.00	130/90/180	−0.349	0.006	0.217	−0.125
1857	Parkfield	36.10	120.65	6.10	146/89/179	0.006	0.135	0.301	0.442
1857	NW of Wrightwood	34.52	118.04	6.30	313/88/−178	–	0.008	0.257	–
1858	San Bernardino Region	34.00	117.50	6.00	321/90/180	−0.210	0.364	0.220	0.374
1860	NW of Parkfield	36.35	120.95	6.00	145/88/180	0.086	0.208	0.142	0.435
1862	San Diego Region	32.70	117.20	6.20	336/90/180	0.007	0.025	0.129	0.160
1872	Owens Valley Region	37.00	118.20	6.30	340/80/−171	−0.003	0.028	0.108	0.132
1875	Imperial Valley Region	32.50	115.50	6.20	327/90/180	0.014	0.239	1.446	1.700
1881	NW of Parkfield	36.10	120.60	6.00	146/89/180	0.255	0.022	0.474	0.751
1883	Santa Barbara Chan. (T)	34.20	119.90	6.30	136/68/105	−0.092	0.007	0.049	−0.036
1885	S. Diablo Range (T)	36.57	120.65	6.40	132/25/101	−0.004	0.033	−0.108	−0.080
1890	San Jacinto Region	33.40	116.30	6.30	125/90/180	0.034	−0.034	0.921	0.921
1891	Near Victoria BC	32.00	115.00	6.00	138/87/−179	0.006	0.026	0.818	0.851
1892	San Jacinto Region	33.20	116.20	6.30	135/90/180	0.032	0.014	1.211	1.258
1894	Near Wrightwood	34.30	117.60	6.20	125/90/180	–	0.049	0.403	–
1894	San Diego Region	32.80	116.80	6.10	137/90/179	−0.028	0.913	0.126	1.010
1896	Owens Valley Region	36.70	118.30	6.30	345/90/180	–	0.042	0.127	–
1899	Near Wrightwood	34.30	117.50	6.40	125/90/180	–	0.020	0.322	–
1901	Parkfield	36.00	120.50	6.40	327/90/180	0.437	0.728	0.638	1.803
1905	S. Diablo Range (T)	36.50	120.60	6.10	295/62/97	−0.012	0.027	−0.232	−0.217
1906	Imperial Valley Region	32.90	115.50	6.20	327/90/180	0.071	0.059	2.074	2.204
1908	Death Valley Region	36.00	117.00	6.00	339/84/177	−0.047	0.221	0.141	0.316
1910	Glen Ivy Hot Springs	33.70	117.40	6.00	128/90/180	−0.277	−0.078	0.403	0.049
1915	Imperial Valley	32.80	115.50	6.00	327/90/180	0.222	0.182	2.442	2.846
1916	SE of Kern County	34.90	118.90	6.00	316/76/166	–	0.181	0.655	–
1922	Parkfield	36.00	120.50	6.00	327/90/180	0.437	0.804	0.789	2.030
1923	San Bernardino Region	34.00	117.30	6.20	320/85/180	−0.062	0.272	0.502	0.712
1925	Santa Barbara (T)	34.30	119.80	6.30	136/68/105	−0.132	0.252	0.118	0.238
1933	Long Beach	33.62	117.97	6.40	315/80/−170	−0.052	−0.233	0.271	−0.014
1934	Parkfield	35.80	120.33	6.10	327/90/180	2.128	0.057	1.662	3.846
1937	San Jacinto Region	33.41	116.26	6.00	309/83/−136	0.040	0.136	1.125	1.302
1942	Fish Creek Mountains	32.97	116.00	6.30	331/80/178	0.096	0.104	1.016	1.216
1946	Walker Pass (T)	35.73	118.06	6.00	346/45/−117	−0.071	0.201	0.062	0.192
1948	Desert Hot Springs	33.93	116.38	6.00	305/70/165	0.019	−0.037	1.209	1.191
1952	Kern County (T)	35.00	119.00	6.40	74/75/50	–	−0.112	−1.519	–
1952	Kern County (T)	35.37	118.58	6.10	74/75/50	–	−1.076	−0.539	–
1952	Bakersfield	35.38	118.85	6.10	333/90/180	−0.717	0.035	0.187	−0.495
1952	Bryson	35.73	121.20	6.00	309/66/144	−0.065	−0.027	0.406	0.313
1954	Arroyo Salada	33.28	116.18	6.40	307/85/175	0.057	0.045	1.846	1.948
1966	Parkfield	35.92	120.53	5.60	147/90/160	0.447	0.107	1.098	1.653
1979	Imperial Valley	32.61	115.32	6.40	136/39/180	–	0.059	2.192	–
1980	Near Victoria Falls	32.19	115.08	6.39	322/90/180	–	0.446	2.117	–
1983	Coalinga (T)	36.24	120.26	6.40	150/15/90	−0.004	−0.127	−0.138	−0.269
1985	Kettleman Hills (T)	36.15	120.05	6.14	138/10/105	−0.169	−0.006	0.283	0.109
1986	Desert Hot Springs	34.00	116.61	6.08	294/37/156	0.096	−0.149	0.819	0.766
1987	Laguna Salada Region	33.09	115.79	6.10	125/90/180	−0.281	0.175	1.425	1.319
1992	Joshua Tree	33.96	116.32	6.22	171/89/−177	−0.048	0.130	1.902	1.984
1993	Owens Valley (T)	36.68	118.10	6.17	210/30/−93	–	−0.060	0.201	–
2004	Parkfield	35.81	120.37	6.04	321/72/−178	1.480	0.217	2.148	3.846

over the past two centuries resolve themselves on an additional 53 $6.0 \leq M_w < 6.5$ events (Table 2, gray focal mechanisms in Fig. 1) (Kagan *et al.* 2006). We do not consider how these smaller events subsequently influence the regional stress field as they only perturb the stress locally (10s of km). Our study focuses on the evolution of stress on the broad landscape of southern California and how the hypocenters of historic quakes have been influenced by these stress changes.

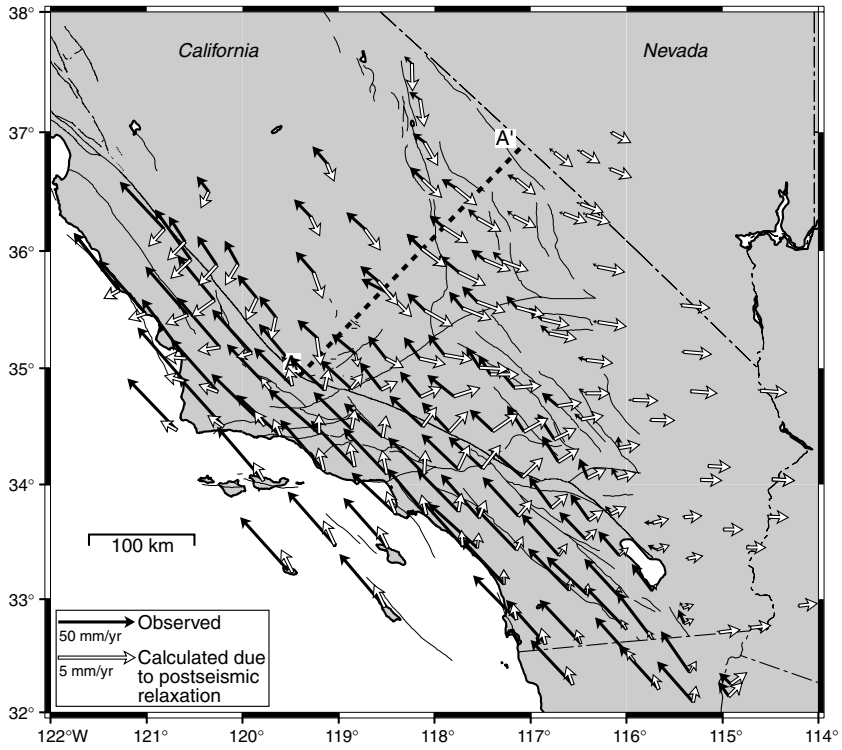

Figure 2. SCEC 3 observed surface velocities and calculated velocities in 2003 based on postseismic relaxation from historic earthquakes (Table 1, but not 1992, 1999, and 2003 events). Note that the observed velocities are plotted on a scale that is 10 times bigger than the postseismic relaxation velocities. For clarity, only a subset of the SCEC 3 velocity set is shown.

2 INTERSEISMIC STRAIN ACCUMULATION

Interseismic strain rates have previously been calculated by Jackson *et al.* (1997) from the first version of the SCEC velocity field (287 velocity vectors), finding that high shear strain rates were observed not only near the major faults, but also in regions surrounding previous earthquakes, such as the 1992 Landers, 1979 Imperial Valley and the 1952 White Wolf events. Working with an increased number of GPS stations, Wdowinski *et al.* (2001) utilized the second version of the SCEC velocity field (363 velocity vectors), where most of the data was concentrated around the SAF. They found high interseismic strain rates to be localized along a dozen subparallel segments in a narrow zone around the San Andreas that correlated well with the active geologic fault segments and concentrated zones of microseismicity. High shear strain rates (0.3–0.95 μstrain/yr) were observed northwards and southwards of the SAF's big bend, whereas the big bend itself was characterized by a diffused low magnitude shear strain rate. Here we utilize the third version of the SCEC Crustal Motion Map (http://epicenter.usc.edu/cmm3/), which provides a broader view of surface motions (840 velocity vectors), including the ECSZ, enabling a more regional understanding of interseismic strain rates (Fig. 2; note that for clarity this figure shows only a subset of the observed velocity vectors). The great density of these measurements minimizes errors associated with interpolating strain rates between station locations.

The advantage of directly calculating strain rates from the observed velocity field is that it does not require us to understand and model the mechanics of interseismic strain accumulation. Non-uniqueness of the surface strain rate in defining how stress varies with depth renders this approach reasonable, but not superior to deep-slip or other approaches that can equally explain observed surface velocities. If we superimpose stresses derived from interseismic strain rates with those derived from separate calculations of postseismic relaxation, however, a problem could arise if the velocity field contains substantial contributions from those same relaxation processes. If such is the case, stress changes associated with postseismic relaxation would be exaggerated. The first step in our analysis is thus to determine the extent to which current surface velocities in southern California are influenced by postseismic relaxation associated with earthquakes that have occurred in the past 200 yr. Contributions of pre-1812 postseismic processes to current surface velocities, such as due to a background strain rate associated with repeated earthquake cycles (Savage & Lisowski 1998; Segall 2002; Dixon *et al.* 2003; Johnson & Segall 2004; Hetland & Hager 2005; Kenner & Simons 2005), is of no concern since these contributions will not be duplicated by our postseismic calculations.

Viscoelastic relaxation contributions are calculated using the code Visco1D developed by Pollitz (1997), which is based on the normal mode representation of deformation in a layered spherical Earth with elastic-viscoelastic coupling, including the effects of compressibility and gravitational coupling. Fault segments are modelled as planar rectangular patches of constant strike, dip, rake and slip, spanning the rupture surface of each earthquake. We assume a layered elastic structure as shown in Fig. 3. The primary unknown in these calculations is the assumed viscosity structure. Analyses of postseismic deformation following the 1992 Landers and 1999 Hector Mine earthquakes suggest that after several years of early fast strain rates, the effective viscosity of the southern California lithosphere can be described with an upper mantle viscosity of the order of 10^{19} Pa s and a lower crustal viscosity three times that level (Pollitz *et al.* 2000; Freed & Bürgmann 2004). This

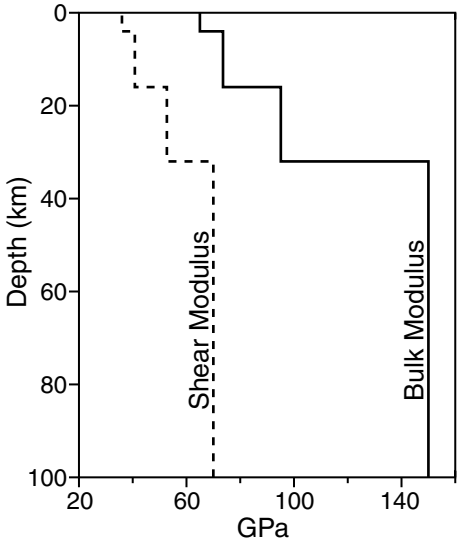

Figure 3. Assumed elastic parameters for our layered Earth model.

is consistent with the effective viscosity of the San Francisco Bay region inferred from observations of postseismic deformation in the decades following the 1906 San Francisco quake (Kenner & Segall 2003; Pollitz & Nyst 2005) and with long-term relaxation times (25 to 40 yr) associated with analytical viscoelastic coupling models associated with the velocity field around the big bend in southern California (Thatcher 1983; Savage & Lisowski 1998). In all of our viscoelastic calculations we use a viscosity of 1.2×10^{19} Pa s for the mantle and 3.6×10^{19} Pa s for the lower crust, the same rheology inferred by Pollitz & Nyst (2005) for the San Francisco region.

Using a constant effective viscosity is an approximation for a viscoelastic rheology that is likely non-linear either due to being a transient rheology (e.g. Pollitz 2003) or a power-law rheology (e.g. Freed & Bürgmann 2004). The time-dependent nature of viscoelastic rheology leads to lower viscosities and higher strain rates immediately after an earthquake, and high viscosities and lower strain rates later on. Assuming a linear rheology will tend to underpredict postseismic strain rates and stress changes early in the process, though the fully relaxed state does not depend on the viscosity assumed. Thus, as most postseismic relaxation processes associated with historic earthquakes are either complete or near completion by 2003 (discussed below), our assumption of linear viscosity does not significantly influence the predicted surface velocities in 2003. Nor does it influence stress changes due to postseismic relaxation, except for perhaps the first 5 yr or so after an event, in which case stress changes would be underpredicted.

The SCEC 3 velocity field had been constructed ignoring the first year and a half after the Landers quake (and all post-Hector Mine data, Shen *et al.* 2003), but postseismic analyses suggest that relaxation continued to influence the velocity field from 1994 to 1999 (Pollitz *et al.* 2000; Freed & Bürgmann 2004). Thus, our initial calculation estimated the average surface velocity due to post-Landers relaxation from 1994 to 1999, which was then removed from the SCEC velocity field. The peak average post-Landers velocity over this time period was found to be as much as 15 mm yr^{-1} within 20 km of the fault and 3 mm yr^{-1} within a 100 km distance, representing a significant portion of the SCEC velocities in the ECSZ. We subtracted these velocities from the SCEC 3 velocity field to form a corrected version more likely representative of long-term interseismic velocities in southern California.

We then calculated the collective contributions from viscoelastic relaxation from 1812 to 2003 earthquakes (Table 1; not including Hector Mine, which is not part of the SCEC data) to southern California surface velocities in 2003. We found these velocities to be relatively small, with peak velocities less than 2 mm yr^{-1}, much smaller than those observed by GPS (note the factor of 10 difference in plotting scales in Fig. 2). In addition, the velocity pattern associated with collective postseismic relaxation shows little correspondence to the observed velocity field. From this we conclude that postseismic relaxation associated with historic earthquakes does not significantly influence the present day velocity field and by extension, has little influence on interseismic strains derived from these velocities.

The predicted velocity field that emerges from calculations of postseismic deformation shows a pattern of dominantly right-lateral strike-slip motion emanating from the SAF. This is consistent with the fact that most significant historic quakes over the past two centuries were right-lateral strike-slip faults along the SAF system. The largest component of the calculated postseismic velocity field is due to continued relaxation from the Fort Tejon quake despite it having occurred 150 yr ago. Fig. 4 shows the calculated influence of postseismic relaxation following the 1857 quake in the years 1860, 1900 and 2003. The pattern of postseismic deformation due to this great quake is continued right-lateral motion, typical following large strike-slip events (e.g. Freed *et al.* 2006). The pattern remains fairly consistent throughout the relaxation process, but the resulting surface velocities drop dramatically with time. Fig. 4b shows SAF fault parallel velocities along a cross-section perpendicular to the SAF. Surface velocities due to postseismic relaxation drop from a

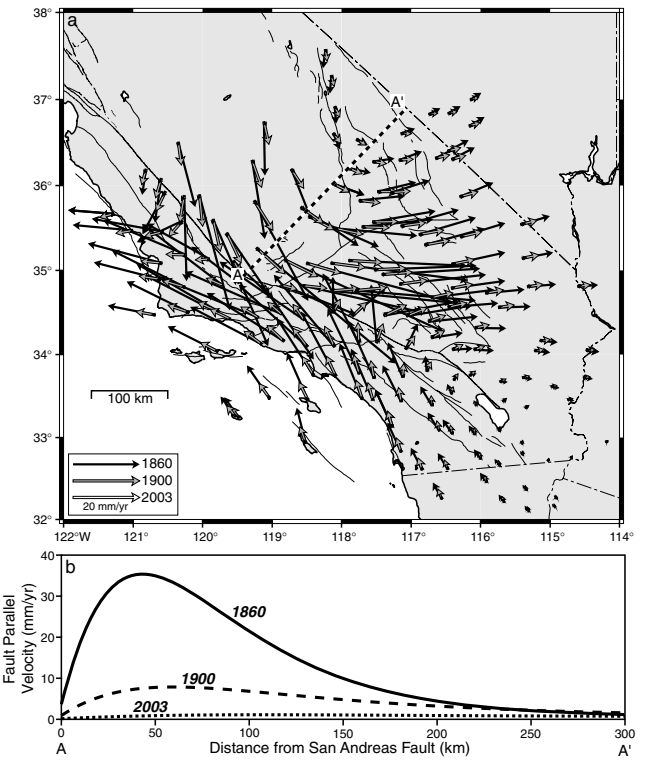

Figure 4. (a) Calculated surface velocities in the years 1860, 1900, and 2003 due to viscoelastic relaxation following the 1857 Fort Tejon quake (velocities in 2003 are "basically invisible" on this scale). (b) Velocities from (a) interpolated along the A-A′ transect.

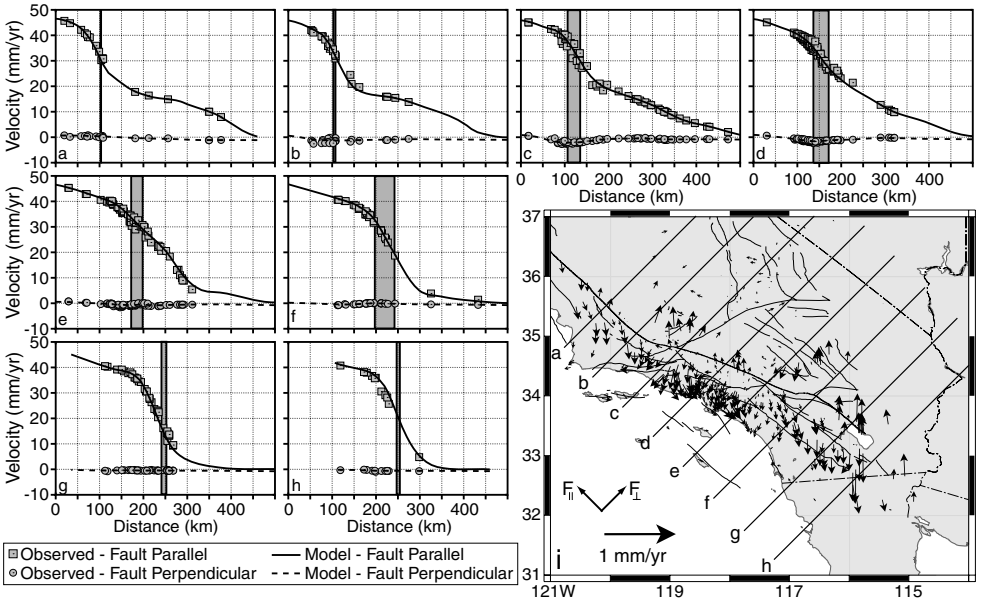

Figure 5. (a–h) SCEC 3 Observed versus interpolated surface velocities (used in strain rate calculations) with 500 km of cross-sections through southern California. (i) Cross-section locations and misfit between observed and interpolated velocities.

maximum of 35 mm yr^{-1} in 1860, to a maximum of 8 mm yr^{-1} in 1900, to only about 1 mm yr^{-1} in 2003.

Having concluded that the SCEC 3 velocity field (minus Landers contributions) does not have a substantial component of postseismic relaxation from events occurring over the past two centuries, we proceeded to calculate associated interseismic strain rates. To calculate interseismic strain rates, each velocity vector was resolved into fault-parallel and fault-perpendicular components, where the fault parallel direction is based on the average azimuth of the SAF (N40°W). We then linearly interpolated the velocity data to an evenly spaced grid with increments of 0.1 degrees across the region using a weighted nearest neighbouring scheme, which dampens any locally sharp velocity contrasts. For grid points outside of the SCEC 3 region, we extrapolated the velocity field based on a fixed North American plate and a Pacific plate with a velocity of 48 mm yr^{-1}. Because of the dense coverage of the SCEC 3 data set, only a few outlying regions required assumptions of relative plate motions. Fig. 5 shows a comparison between observed and interpolated fault parallel and fault perpendicular velocities at eight cross-sections across the region. Residual velocities (which are less than 1 mm yr^{-1}) are shown in Fig. 5(i).

We then triangulate the evenly spaced grid points (with a resolution of 0.1 degrees) using Delaunay triangulation (e.g. Shewchuk 1996), and the strain tensor is determined for each triangle using minimum norm least squares. The resolved maximum shear-strain rate across southern California inferred from the velocity field is shown in Fig. 6. Interseismic shear strain is concentrated along the SAF through southern California, though the San Jacinto Fault shares strain with the SAF in the south. Strain rates along the creeping section of the SAF (above 36°N) are not well resolved because of a lack of stations on the west side of the fault, and below 33°N for similar reasons (creeping segments in these regions also induce anomalous interpretations of strain rate). These results are in general agreement with the magnitude of strain rates inferred from SCEC 1 (Jackson *et al.* 1997) and SCEC 2 (Wdowinski *et al.* 2001), though the present analysis has a substantially larger array of geodetic measurements from which to more accurately infer the strain

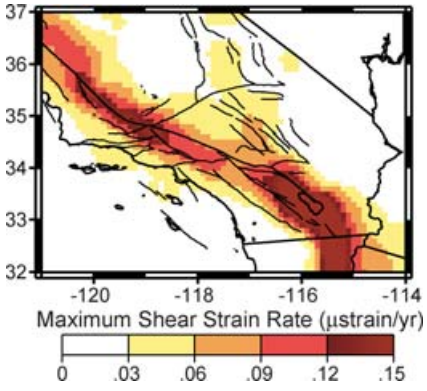

Figure 6. Maximum shear strain rates based on SCEC 3 velocities minus contributions from Landers postseismic relaxation (see text).

field. Relatively high strain rates in the vicinity of the Landers quake may suggest that the contribution to the velocity field due to post-Landers relaxation was probably not completely removed by our correction.

3 THE EVOLUTION OF STRESS

We focus our study on the calculation of Coulomb stress changes, which is based on the concept of a critical Coulomb failure stress, σ_c, in which

$$\sigma_c = \tau - \mu(\sigma_n - p), \tag{1}$$

where τ is shear stress parallel to the slip direction of a fault, σ_n is fault-normal (or clamping) stress, p is pore fluid pressure, and μ is the coefficient of friction (Jaeger & Cook 1979; Scholz 2002). The Coulomb failure criterion was developed in the laboratory where the absolute applied shear and normal stresses on rock specimens could be measured. While the absolute stress field is difficult to determine, as it depends on a long, unknown history of earthquakes and other dynamic processes, stress changes due to

historic coseismic, postseismic and interseismic processes can be estimated. We thus rewrite the equation for Coulomb stress change in the form,

$$\Delta\sigma_c = \Delta\tau - \mu'\Delta\sigma_n, \quad (2)$$

where Δ represents change in stress and μ' is the apparent friction, which takes into account reductions in friction due to pore pressure changes. This equation implies that a fault will be brought closer to failure if the shear stress parallel to the slip vector is increased or the normal stress is decreased (positive change in Coulomb stress), or will be brought further away from failure if these components are of the opposite sign (negative change in Coulomb stress).

Seemingly oversimplified, calculations of coseismic Coulomb stress changes have shown a correspondence with many seismic observations including aftershock distributions, (Reasenberg & Simpson 1992; Hardebeck *et al.* 1998; Toda *et al.* 1998; Parsons *et al.* 1999; Wyss & Wiemer 2000), earthquake sequences (Stein *et al.* 1994; Hodgkinson *et al.* 1996; Nostro *et al.* 1997; Nalbant *et al.* 1998), and the quiescence of broad, normally active regions following large earthquakes (Harris & Simpson 1996). Several earthquake-triggering studies suggest that an increase of less than 0.1–0.3 MPa, which is a small fraction of typical coseismic stress drops, may be sufficient to trigger seismicity, whereas reduction by the same amount may suppress them.

We calculate the evolution of Coulomb stress in southern California by considering contributions from coseismic, postseismic and interseismic stress changes since the 1812 Wrightwood earthquake. Our objective is to determine the role of each of these mechanisms in the evolution of stress since 1812 and to determine how stress at the hypocenters on subsequent earthquake rupture planes were influenced. Several studies suggest that aftershocks of thrust faults are sensitive to normal stress changes, implying a relatively high apparent friction coefficient for thrust faults, perhaps about 0.8 (e.g. Stein & Ekström 1992;Shearer 1997; Hardebeck *et al.* 1998; Parsons *et al.* 1999). In contrast, evidence favours low friction for strike-slip faults with significant cumulative slip, such as the San Andreas, for which $\mu' < 0.4$ (Zoback *et al.* 1987; Harris *et al.* 1995; Parsons *et al.* 1999; Toda & Stein 2002). Correspondingly, our Coulomb stress calculations assume a constant effective friction of $\mu' = 0.8$ when calculating stress changes on thrust faults and of $\mu' = 0.4$ for strike-slip faults. Unless stated otherwise, all of our calculations assume a hypocenter depth of 8 km, the average nucleation depth of the earthquakes considered.

3.1 Coseismic stress changes

Coseismic Coulomb stress changes are calculated for all $M_w \geq 6.5$ events since 1812 (Table 1) based on the method of Pollitz (1996) and slip distributions based on previous analyses (Helmberger *et al.* 1992; Deng & Sykes 1997a, b; Hurst *et al.* 2000; Hardebeck *et al.* 2004; see Table 1 for respective sources). Fig. 7 shows the results of cumulative coseismic Coulomb stress changes as resolved on right-lateral strike-slip faults parallel to the general trend of the SAF (N40°W). This is a reasonable approximation of how most strike-slip faults in the region have been coseismically loaded by previous events. This figure focuses on six time periods: just after the 1812 $M_w = 7.5$ Wrightwood quake (Fig. 7a), just after the 1857 $M_w = 8.2$ Fort Tejon quake (Fig. 7b), just after the 1892 $M_w = 7.2$ Laguna Salada quake (Fig. 7c), just after the 1952 $M_w = 7.5$ Kern County quake (Fig. 7d), just after the 1992 $M_w = 7.3$ Landers quake (Fig. 7e), and the cumulative change in Coulomb stress due to all considered events as of the end of 2005 (Fig. 7f). Given the uncertainty in the friction and pore pressure inherent to faults (e.g. Beeler *et al.* 2000), we also plot coseismic Coulomb stress for the case where $\mu' = 0.0$ (i.e. shear-stress change only) in Supplemental Figure S1.

Fig. 7 shows that the coseismic stress field in southern California is dominated by stress changes imparted by the 1857 Fort Tejon quake, by far the largest event to occur over the past 200 yr Coulomb stress has been increased to the northwest (Parkfield region) and to the southeast where the San Bernardino Mountain and Coachella Valley segments of the SAF and the San Jacinto fault lie. Both of

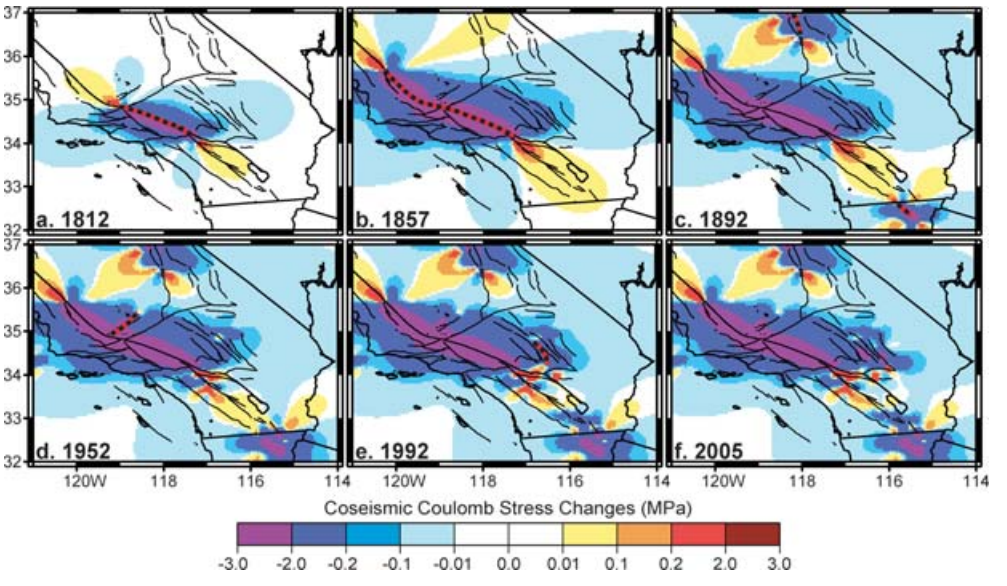

Figure 7. Calculated coseismic Coulomb stress changes resolved at 8 km depth on vertical right-lateral strike-slip faults striking parallel to the San Andreas fault (N40°W) with apparent friction $\mu' = 0.4$ at various times over the past two centuries: just after the (a) 1812 $M_w = 7.5$ Wrightwood quake, (b) 1857 $M_w = 8.2$ Fort Tejon quake, (c) 1892 $M_w = 7.2$ Laguna Salada quake, (d) 1952 $M_w = 7.5$ Kern County quake, (e) 1992 $M_w = 7.3$ Landers quake, and (f) cumulative change in Coulomb stress due to all considered events as of the end of 2005. Each panel shows the major earthquake rupture surface (black and red dashed line) that occurred that year (none for 2005).

these regions are marked by a large number of events since 1857. The 1857 quake also led to a stress shadow (region of Coulomb stress decrease) for similarly aligned faults to the west and east of the rupture zone, most notably across the southern portion of the Eastern California Shear Zone. The 1872 Owens Valley rupture further to the north along the ECSZ lies in an area of small positive stress change. The stress shadow may explain why few events have occurred in the southern ECSZ from 1857 until the recent events of the 1990s, but faults in the ECSZ also have long (thousands of years) recurrence intervals (Rockwell *et al.* 2000) and therefore the recent lack of large events may not be remarkable. Unlike the documented reduction of seismicity within the stress shadow induced by the 1906 San Francisco quake (Bakun 1999), seismicity in the ECSZ prior to the 1857 event is not well constrained. Thus, it is difficult to draw firm conclusions regarding the significance of the Fort Tejon stress shadow. The cumulative effect of coseismic Coulomb stress changes (at 8 km depth) over the past two centuries is stress relief over 79% of southern California, compared to stress increases over 21% of the region.

We have calculated the coseismic Coulomb stress change as resolved on the sense of hypocentral slip (Table 1, column 6; Table 2, column 6) for each historic earthquake over the past two centuries. The cumulative coseismic stress change for each event just before rupture due to all previous events is summarized in Table 1 (column 8) and Table 2 (column 7). Coseismic Coulomb stress changes could not be accurately calculated at several events as they occurred very close to previous rupture surfaces and calculated stress changes vary greatly with small variations in model parameters, as indicated with dashed lines in Table 1 and 2. A summary of these tables finds that 56% of hypocenters experienced an increase in Coulomb stress due to coseismic slip of earlier events. This percentage supports the argument that earthquake occurrence is controlled by factors other than coseismic Coulomb stress changes alone. This conclusion is consistent with the findings of Kagan *et al.* (2005). Deng & Sykes (1997a,b) did not analyze coseismic stress changes alone.

Fig. 8 (black dashed lines) shows how coseismic Coulomb stress changes track with time for each of the hypocenters listed in Table 1 (tracked changes for Table 2 events are shown in Supplemental Figure S2). This figure shows that in general the 1812 Wrightwood, 1857 Fort Tejon, 1892 Laguna Salada and 1940 Imperial Valley had the most influence on stress changes at subsequent hypocenters due to the combination of earthquake magnitude and proximity to later events. For example, coseismic Coulomb stress at the hypocenter of the 1952 Kern County earthquake was significantly increased by the 1812 Wrightwood and 1857 Fort Tejon quakes, but not strongly influenced by other events. Stress at the hypocenter of the 1968 Borrego Mountain earthquake was increased by the 1812 Wrightwood, 1857 Fort Tejon, 1892 Laguna Salada and 1940 Imperial Valley quakes. Stress at the hypocenter of the 1992 Big Bear quake was decreased by the 1812 Wrightwood, 1857 Fort Tejon and the 1899 and 1915 San Jacinto quakes. Stress at the Big Bear hypocenter was then increased by the 1992 Landers quake only 3 hr before its rupture, though not by a sufficient quantity to overcome the preceding coseismic stress decreases. Coseismic Coulomb stress at the 1915 Volcano Lake hypocenter was greatly diminished by the nearby 1892 Laguna Salada quake, yet still ruptured less than two decades later. Such occurrences strongly suggest that the timing of many southern California events is due to factors other than the magnitude of coseismic Coulomb stress change.

3.2 Postseismic stress changes

Following large earthquakes, coseismic stress changes are further modified by relaxation of a viscous lower crust and upper mantle, which serves to transfer stress from these warm regions both upwards to the seismogenic crust and outwards across a broader region. Calculations of postseismic stress changes were carried out using the same numerical code and assumptions discussed in Section 2. The influence of postseismic relaxation of a viscoelastic lower crust and upper mantle on Coulomb stress changes associated with right-lateral strike-slip faults parallel to the SAF is shown in Fig. 9. (Supplemental Figure S3 show these time frames for an assumed frictional values of $\mu' = 0$.) A comparison of coseismic (Fig. 7) and postseismic (Fig. 9) Coulomb stress changes shows that both fields are dominated by the 1857 Fort Tejon quake with both mechanisms leading to stress increases at the ends of the Fort Tejon rupture and stress decreases to either side for strike-slip events parallel to the SAF. In general, postseismic stress changes further intensify and widen coseismic stress changes, but rapidly rebuilds stress along rupture planes. Table 1 (column 9) and Table 2 (column 8) summarize the postseismic Coulomb stress changes due to relaxation associated with previous events imparted at the hypocenter of each earthquake. A summary of these tables finds that 73% of hypocenters experienced an increase in postseismic Coulomb stress, showing a modestly greater correlation between postseismic Coulomb stress increases and the location of subsequent hypocenters than was observed in the coseismic calculations.

Fig. 10 shows the combined influence of coseismic and postseismic Coulomb stress changes on right-lateral strike-slip faults parallel to the SAF (Supplemental Figure S4 show these time frames for zero friction). As expected from the discussion above, the addition of postseismic stress changes greatly magnifies the coseismic stress changes to the northwest and southeast of the Fort Tejon rupture and greatly increases the magnitude and extent of the stress shadow imparted by the Fort Tejon quake, especially over the ECSZ. (see also Pollitz & Sacks 1992; Rydelek & Sacks 2001). Postseismic stress changes lead to a decrease in the area of reduced Coulomb stress (at 8 km depth) from 79% associated with coseismic stress changes alone to 69% within the study region when postseismic stress changes are also taken into account.

Fig. 8 (solid grey lines) shows how combined coseismic and postseismic Coulomb stress changes track with time for each of the hypocenters listed in Table 1 (tracked postseismic changes for Table 2 events are shown in Supplemental Figure S2). This figure shows that in most cases postseismic stress changes tended to greatly increase coseismic stress changes (for reasons discussed above). In some cases, such as the 1994 Northridge and 2003 San Simeon hypocenters, postseismic stress changes from previous events were an order of magnitude greater than their coseismic effects. For several hypocenters (including the 1858, 1872 (the aftershock), 1885, 1894, 1905, 1908, 1923, 1925, 1946, 1992 and 2003 events), postseismic relaxation modifies coseismic Coulomb stress decreases to net (coseismic plus postseismic) stress increases. But for others (including the 1855, 1883, 1915 (Volcano Lake), 1952c, 1987, 1992b), positive postseismic Coulomb stress changes did not make up for coseismic stress decreases. Whereas 56% of the hypocenters of events listed in Tables 1 and 2 were pushed closer to failure by coseismic stress increases, 70% were pushed closer to failure by consideration of the cumulative effect of coseismic and postseismic Coulomb stress changes.

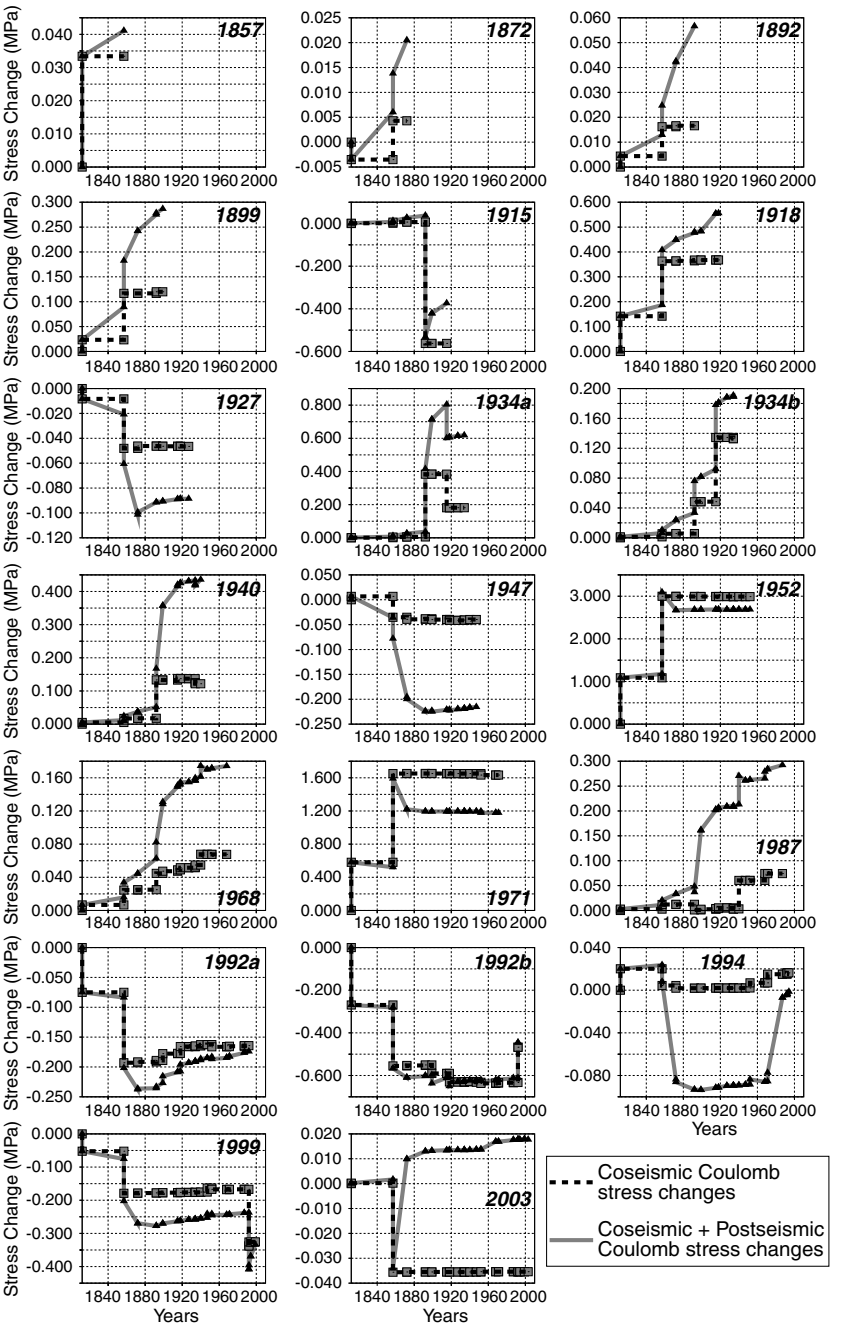

Figure 8. Coseismic and net coseismic plus postseismic Coulomb stress changes from just before the 1812 Wrightwood earthquake to just before rupture as a function of time for each hypocenter listed in Table 1.

Amongst the larger events, the occurrence of the 1947 Manix, 1992 Landers, 1992 Big Bear and the 1999 Hector Mine earthquakes remain difficult to explain in terms of net Coulomb coseismic and postseismic stress changes, as the respective hypocenters all experience net coseismic plus postseismic Coulomb stress decreases, primarily from the Fort Tejon stress shadow. It is not clear whether coseismic changes associated with the Landers quake encouraged or inhibited rupture of the Hector Mine earthquake, as slight changes in modelling assumptions can flip the sign of coseismic stress changes (see also Harris & Simpson 2002). Postseismic relaxation following the Landers earthquake does, however, increase Coulomb stress at the hypocenter of the Hector Mine event by ∼0.08 MPa (see also Freed & Lin 2001; Zeng 2001; Pollitz & Sacks 2002). Despite the fact that this postseismic stress increase associated with the Landers quake is not sufficient to overcome the stress shadow induced by the 1857 earthquake, the Hector Mine ruptured only 7 yr after the Landers quake. Again, this raises the possibility that the rate of Coulomb stress change may be more important than the magnitude (Parsons *et al.* 2000; Toda *et al.* 2005).

3.3 Interseismic stress changes

Interseismic Coulomb stress change rate was calculated based on the inferred interseismic strain rate (Fig. 6) using the time derivative of equations 3–1 to 3–3 in Turcotte & Schubert (2002). Fig. 11 shows

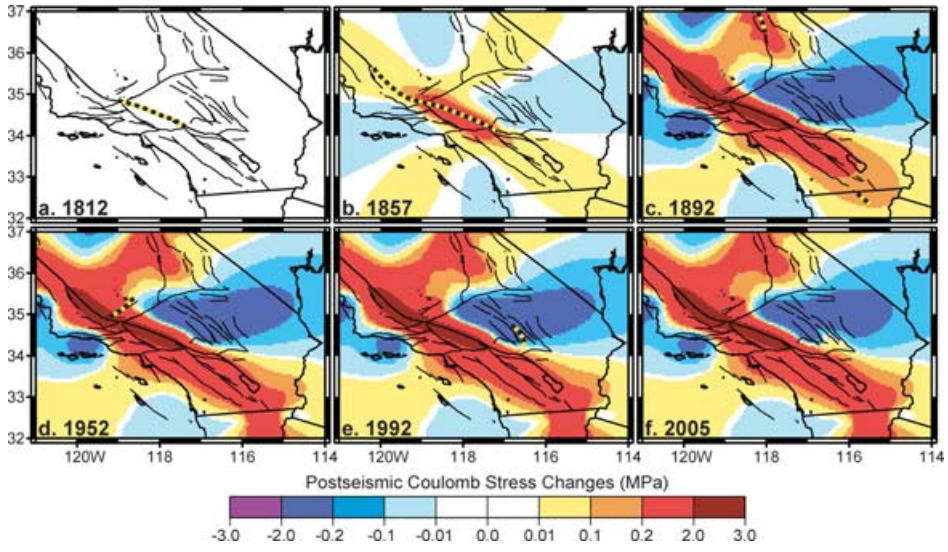

Figure 9. Same as Fig. 7, but for calculated postseismic Coulomb stress changes.

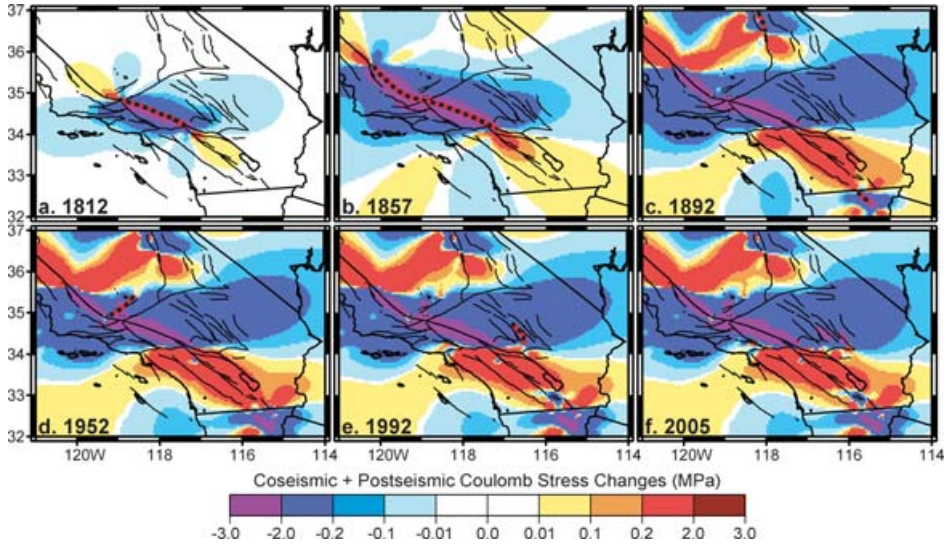

Figure 10. Same as Fig. 7, but for calculated coseismic plus postseismic Coulomb stress changes.

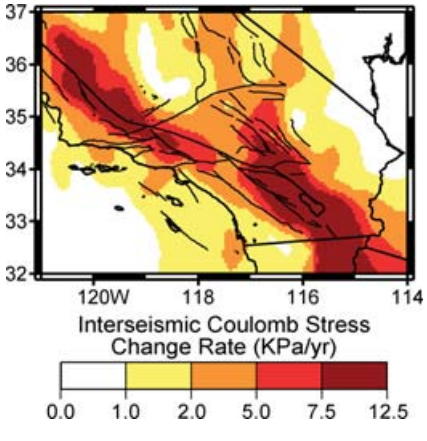

Figure 11. Interseismic Coulomb stress rates resolved on vertical right-lateral strike-slip faults striking parallel to the San Andreas fault (N40°W). Calculations are based on an assumed effective friction of 0.4 and are derived from the shear strain field shown in Fig. 6.

the resulting interseismic Coulomb stress rate for right-lateral strike-slip faults striking parallel to the SAF (N40°W). Peak stressing rates of >2 KPa yr^{-1} across a band $\sim$200 km wide along the SAF is consistent with differential stresses found by Parsons (2006), who used GPS velocities to drive a model of crustal deformation. This band is much broader and the magnitude of stressing rates much lower than that found from models of loading due to deep slip (e.g. Smith & Sandwell 2003, 2006). As pointed out by Parsons (2006), either modelling approach can satisfy surface velocity constraints, thus leaving the actual mechanisms of strain accommodation unknown.

The pattern of the regional stressing rate closely resembles the maximum shear strain rate. As interseismic shear represents the driving load of the SAF system, it is not surprising that the interseismic Coulomb stress rate is only positive. Shear stress rates are maximized along the Cholame and Mojave segments of the SAF in the north and along the Coachella Valley segment and the San Jacinto fault in the south, with the presence of the big bend causing a broadening of the high-stress zone to encompass the ECSZ through the middle of the region. Though these rates are relatively

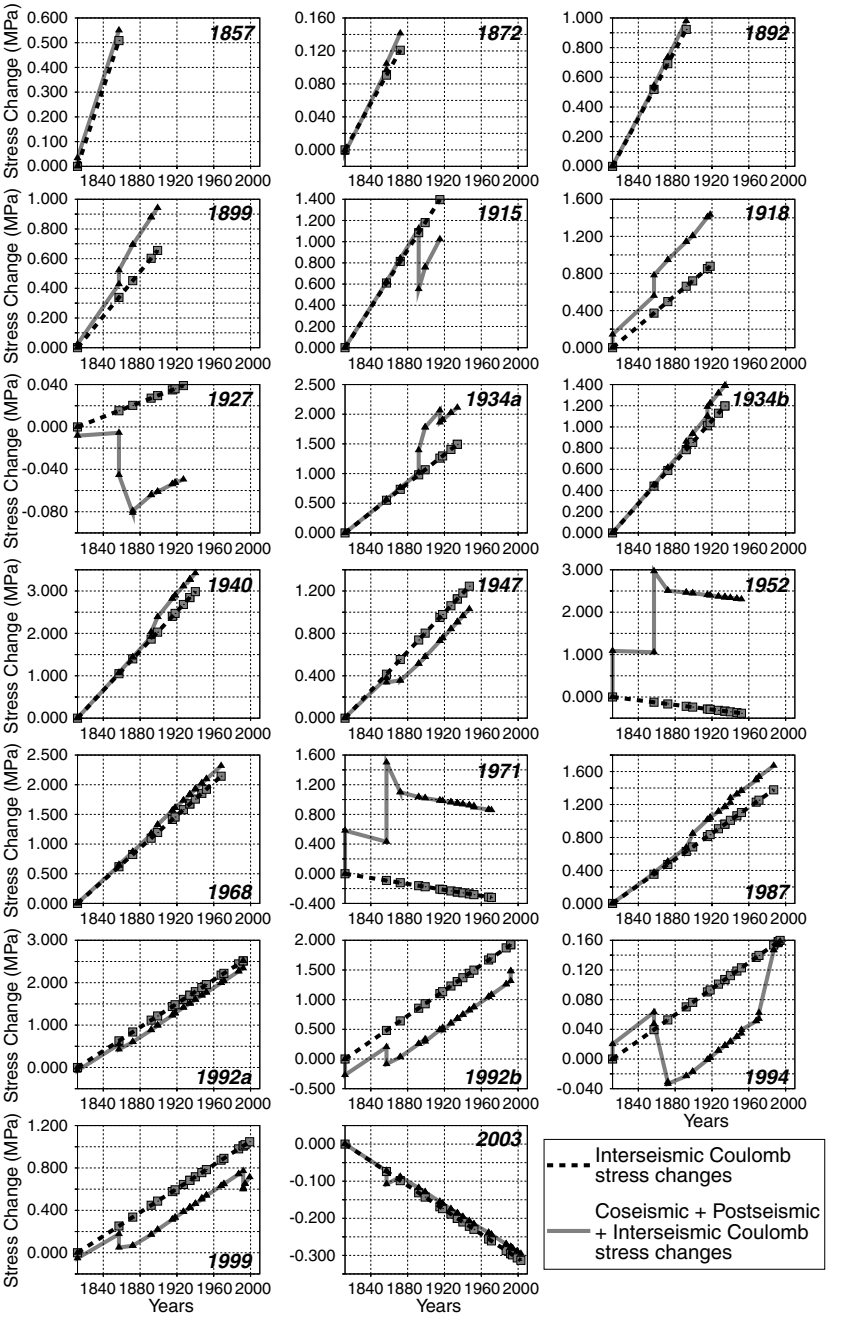

Figure 12. Interseismic and net (coseismic plus postseismic plus interseismic) Coulomb stress changes from just before the 1812 Wrightwood earthquake to just before rupture as a function of time for each hypocenter listed in Table 1.

small on a yearly basis compared to stress changes induced by earthquakes, their relentless application dominates the stress field in the long term. The interseismic stress rate calculations are inaccurate at the creeping sections of the SAF to the north of 36°N and south of 32.5°N. Both of these regions are marked by a sharp discontinuity in the strain rate field, which are not captured by the strain field we derived from the sparsely distributed GPS observations.

Fig. 12 (dashed lines with squares) shows how interseismic Coulomb stress changes track with time for each of the hypocenters listed in Table 1 (tracked changes for Table 2 events are shown in Supplemental Figure S5). Table 1 (column 10) and Table 2 (column 9) show the total change in Coulomb stress from 1812 to the time of rupture due to interseismic loading for each hypocenter. While one may expect to find that Coulomb stress is increased at all hypocenters due to interseismic loading, as one would surmise that all faults in southern California arise from the long term motions of the Pacific and North American plates, that is not the case for several thrust events, including the 1952 Kern County and 1971 San Fernando hypocenters that are calculated to be unloaded by the interseismic stressing rate we deduced from the GPS velocities. These hypocenters were, however, both significantly loaded coseismically by the 1857 Fort Tejon quake to the extent that the net Coulomb stress change since 1812 at each of these hypocenters is positive. If these calculations are correct, it would suggest that both events are responses to Fort Tejon type events on the SAF, as opposed to the interseismic stress changes. For thrust event such as

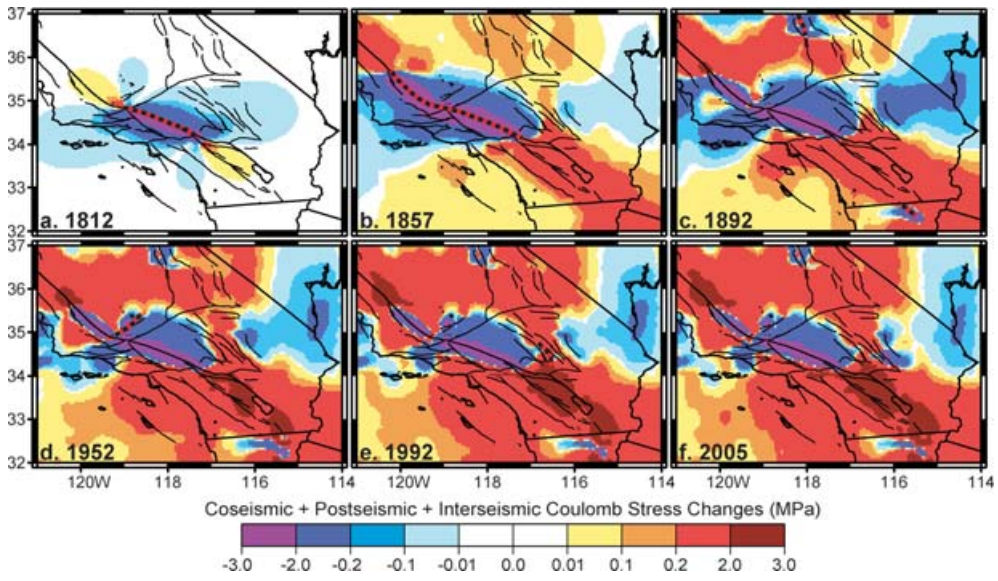

Figure 13. Same as Fig. 7, but for calculated coseismic plus postseismic plus interseismic Coulomb stress changes.

these the assumption of an apparent friction (in this case 0.8) greatly influences calculated interseismic Coulomb stress changes. In fact, Coulomb stresses at the hypocenters of both of these events is calculated to increase in response to interseismic loading if the apparent friction is assumed to be low (<0.4). This is also true for the loading of the hypocenters of the 1983 Coalinga and 2003 San Simeon events.

3.4 Net stress changes

Assuming a neutral stress state just prior to the 1812 Wrightwood earthquake, we added interseismic stress (stress rate multiplied by time since 1812) to that calculated from coseismic and postseismic stress changes, providing a view of the net evolution of stress through the 19th and 20th centuries in southern California (Fig. 13) (Supplemental Figure S6 shows net stress changes for zero apparent friction). The addition of interseismic stresses increase stress throughout the region for strike-slip faults similarly oriented to the SAF. Interseismic stress increases add to large positive coseismic and postseismic stress along the southern portion of the SAF system (southeast of the Fort Tejon rupture), generating a region of significant unrelieved stress since 1812. This evolution has critically loaded the San Bernardino Mountain and Coachella Valley segments of the SAF and the San Jacinto Fault. Stress on the southernmost San Andreas segment, which has not ruptured since ~1680 (Sieh *et al.* 1989), has increased on the order of 3 MPa due to coseismic, postseismic and interseismic stress changes since 1812 (Fig. 13f). Due to interseismic stress rates alone, stress on this segment has increased by more than 5 MPa since the last rupture in 1680. Despite the fact that this southern region is the most seismically active in southern California over the past 100 yr, with more than two dozen $M_w \geq 6.0$ events, this seismicity has done little to relieve the stress that has developed both from interseismic loading and the 1857 Fort Tejon earthquake and subsequent postseismic relaxation.

In contrast, interseismic stress increases have worked to erode the large stress shadow cast by the 1857 Fort Tejon quake over the ECSZ (compare Figs 10f and 13f). The result is a reduction of the area within southern California characterized by a post-1812 decrease in Coulomb stress from 69% for coseismic plus postseismic changes, to only 34% after interseismic loading is considered. At current interseismic rates, the stress shadow cast by the Fort Tejon quake and associated postseismic relaxation should be erased within the next several decades. If this shadow has been responsible for decreased seismicity in this portion of the ECSZ, then this region may experience a significant increase in seismicity in the decades to come. Though it is only speculation, it is possible that the quakes that occurred in the southernmost ECSZ in the 1990s (Joshua Tree, Landers, Big Bear, Hector Mine) could mark a beginning of a new cycle of seismicity in the region. Interseismic stress increases are also working to reload the Fort Tejon rupture surface, though it will take more than another century for the stress levels on this segment of the SAF to reach pre-1812 levels.

Fig. 12 (grey lines with triangles) shows how the combined coseismic, postseismic and interseismic Coulomb stress changes track with time for each of the hypocenters listed in Table 1 (tracked changes for Table 2 events are shown in Supplemental Figure S5). Table 1 (column 11) and Table 2 (column 10) show the net change in stress from 1812 to the time of rupture due for each earthquake considered. As expected, most events experience a net Coulomb stress increase. Several earthquakes in our catalogue appear to nucleate despite their hypocenters having experienced a net Coulomb stress decrease between 1812 and the time of their rupture. These include the 1927 Lompoc, the 1952 Bakersfield, the 1983 Coalinga, the 2003 San Simeon and several small 19th century events. Almost all of these exceptions are thrust events. As discussed above, the stresses at these hypocenters are very sensitive to assumptions of apparent friction. With the exception of a couple of early 19th century events (1827, 1855), where slip characteristics are not well constrained, the 1952 Bakersfield quake is the only modern day strike-slip event to have occurred with a net decrease in Coulomb stress. The 1952 Bakersfield earthquake was an aftershock of the Kern County earthquake, occurring only 8 hr after the main shock despite a calculated decrease in Coulomb stress due to the Kern County rupture. The rake of this earthquake, which has a significant influence on resolved stresses at the hypocenter, is poorly resolved, which could account for this discrepancy. Choosing the northeast-striking nodal plane leads to a positive coseismic Coulomb stress

change as well. It is also possible that another mechanism such as dynamic triggering may have played a role in the triggering of this aftershock.

4 CONCLUSIONS

We calculated the evolution of Coulomb stress in southern California due to $M_w \geq 6.5$ earthquakes since 1812 due to interseismic strain accumulation, coseismic slip and postseismic relaxation of a viscoelastic lower crust and upper mantle. The calculations reveal the overwhelming influence of the 1857 $M_w = 8.2$ Fort Tejon earthquake on the evolving stress field of southern California. Stress changes associated with this earthquake cast a wide stress shadow decreasing the load on faults in the region throughout the 19th century, while greatly increasing stresses to the north (Parkfield region) and the southern SAF system to the south. These stress changes were greatly enhanced by subsequent postseismic relaxation through the beginning of the 20th century. Interseismic stress accumulation further increased loading on most of the strike-slip faults in southern California, adding to stress increases from coseismic and postseismic stress changes, and working to erode the stress shadow in the ECSZ. Postseismic relaxation also occurs on a smaller scale following each earthquake, though only the $M_w \geq 7$ events significantly influence the regional distribution of stress. Today southern California is characterized by unrelieved stress increases along the San Bernardino Mountain and Coachella Valley segments of the SAF and the San Jacinto fault zone.

Our results demonstrate the importance of postseismic viscoelastic relaxation in the redistribution of stress following large earthquakes, but also reveal that such processes are near completion and thus do not significantly influence the regional velocity field presently observed in southern California. Calculations show that, with the exception of the 1992 Landers and 1994 Hector Mine quakes, postseismic relaxation of previous quakes over the past two centuries account for less than 2 mm yr^{-1} of currently observed surface velocities.

We also calculated the evolution of Coulomb stress at the hypocenter of $M_w \geq 6$ earthquakes since 1812. We found that coseismic Coulomb stress changes increased the stress at 56% of subsequent historic hypocenters, indicating that earthquake occurrence is not uniquely determined by coseismic stress changes. This percentage rises to 70% when postseismic stress changes are also considered. Not surprisingly, interseismic stress accumulation is found to load most faults in the region, but not all. Some hypocenters, such as those associated with the 1952 Kern County and 1971 San Fernando quakes, are modestly unloaded by interseismic strains used in our model calculation. These results could arise from our assumption of high apparent friction on thrust faults, limitations that arise from inferring strain from a limited set of GPS velocities, or they could imply that such events only occur in response to the manner in which major events such as the 1857 Fort Tejon quake reorganize the stress field. Incorporating interseismic loading in the stress-change calculations modestly increases the percentage of events that experienced Coulomb-stress increase since 1812 to 73%.

While most historic earthquakes in southern California incurred Coulomb stress increases due to prior earthquakes that occurred since 1812, this finding does not prove that fault-interaction stresses play a dominant role in the distribution of earthquakes in space and time. Nonetheless, we believe it is appropriate to incorporate knowledge about the evolution of stress derived from physical models of interseismic, coseismic and postseismic deformation into time-dependent earthquake hazard estimates of active fault systems.

ACKNOWLEDGMENTS

We thank Bob Simpson and Ross Stein for their insightful reviews that helped us greatly improve the focus and quality of the manuscript.

REFERENCES

Bakun, W.H., 1999. Seismic activity of the San Francisco Bay region, *Bull. Seismol. Soc. Am.,* **89,** 764–784.

Beeler, N.M., Simpson, R.W., Hickman, S.H. & Lockner, D.A., 2000. Pore fluid pressure, apparent friction, and Coulomb failure, *J. Geophys. Res.,* **105**(B11), 25 533–25 542.

Chéry J., Merkel, S. & Bouissou, S., 2001. A physical basis for time clustering of large earthquakes, *Bull Seismo. Soc. Am.,* **91**, 1685–1693.

Deng, J. & Sykes, L.R., 1997a. Evolution of the stress field in southern California and triggering of moderate-size earthquakes: a 200-year perspective, *J. Geophys. Res.,* **102,** 9859–86.

Deng, J. & Sykes, L.R., 1997b. Stress evolution in southern California and triggering of moderate-, small-, and micro-size earthquakes, *J. Geophys. Res.,* **102,** 24 411–24 435.

DeMets, C. & Dixon, T., 1999. New kinematic models for Pacific-North America motion from 3 Ma to present, 1: evidence for steady motion and biases in the NUVEL-1A model, *Geophys. Res. Lett.,* **26,** 1921–1924.

Dixon, T.H., Norabuena, E. & Hotaling, L., 2003. Paleoseismology and Global Positioning System; earthquake-cycle effect and geodetic versus geologic fault slip rates in the Eastern California Shear Zone, *Geology,* **31,** 55–58.

Felzer, K.R. & Brodsky, E.E., 2005. Testing the stress shadow hypothesis, *J. Geophys. Res.,* **110,** B05S09, doi:10.1029/2004JB003277.

Felzer, K.R. & Brodsky, E.E., 2006. Decay of aftershock density with distance indicates triggering by dynamic stress, *Nature,* **441,** 735–738.

Freed, A.M., 2005. Earthquake triggering by static, dynamic, and postseismic stress transfer, *Annu. Rev. Earth Planet. Sci.,* **33,** 335–367.

Freed, A.M. & Bürgmann, R., 2004. Evidence of power-law flow in the Mojave desert mantle, *Nature,* **430,** 548–551.

Freed, A.M. & Lin, J., 1998. Time-dependent changes in failure stress following thrust earthquakes, *J. Geophys. Res.,* **103,** 24 393–24 409.

Freed, A.M., & Lin, J., 2001. Delayed triggering of the 1999 Hector Mine earthquake by viscoelastic stress transfer, *Nature,* **411,** 180–183.

Freed, A.M. & Lin, J., 2002. Accelerated stress buildup on the southern San Andreas Fault and surrounding regions caused by Mojave Desert earthquakes, *Geology,* **30,** 571–574.

Freed, A.M., Bürgmann, R., Calais, E., Freymueller, J. & Hreinsdóttir, S., 2006. Implications of Deformation Following the 2002 Denali, Alaska Earthquake for Postseismic Relaxation Processes and Lithospheric Rheology, *J. Geophys. Res.,* **111,** B01401, doi:10.1029/2005JB003894.

Gomberg, J., 1996. Stress/strain changes and triggered seismicity following the M_w 7.3 Landers, California earthquake, *J. Geophys. Res.,* **101,** 751–764.

Gomberg, J., Bodin, P., Larson, K. & Dragert, H., 2004. Earthquake nucleation by transient deformations caused by the M = 7.9 Denali, Alaska, earthquake, *Nature,* **427,** 621–624.

Hardebeck, J., Nazareth, J. & Hauksson, E., 1998. The static stress change triggering model; constraints from two southern California aftershock sequences, *J. Geophys. Res.,* **103,** 24427–37.

Hardebeck, J.L., Boatwright, J., Dreger, D. *et al.*, 2004. Preliminary report on the 22 December 2003 M6.5 San Simeon, California earthquake, *Seismol. Res. Lett.,* **75**(2), 155–172.

Harris, R.A., 1998. Introduction to special section: stress triggers, stress shadows, and implications for seismic hazard, *J. Geophys. Res.,* **103,** 24 347–24 358.

Harris, R.A. & Simpson, R.W., 1998. Suppression of large earthquakes by stress shadows: a comparison of coulomb and rate-and-state failure, *J. Geophys. Res.,* **103,** 24 439–24 451.

Harris, R.A. & Simpson, R.W., 2002. The 1999 M-w 7.1 Hector Mine, California, earthquake: a test of the stress shadow hypothesis?, *Bull. Seismol. Soc. Am.,* **92,** 1497–1512.

Harris, R.A. & Simpson, R.W., 1996. In the shadow of 1857-the effect of the great Ft. Tejon earthquake on subsequent earthquakes in southern California, *Geophys. Res. Lett.,* **23,** 229–232.

Harris, R.A., Simpson, R.W. & Reasenberg, P.A., 1995. Influence of static stress changes on earthquake locations in southern California, *Nature*, **375,** 221–224.

Heaton, T.H., 1982. The 1971 San Fernando Earthquake—a double event, *Bull. Seis. Soc. Am.,* **72,** 2037–2062.

Helmberger, D.V., Somerville, P.G. & Garnero, E., 1992. The location and source parameters of the Lompoc, California, Earthquake of 4 November 1927, *Bull. Seismol. Soc. Am.,* **82,** 1678–1709.

Hetland, E.A. & Hager, B.H., 2005. Postseismic and interseismic displacements near a strike-slip fault: a two-dimensional theory for general linear viscoelastic rheologies, *J. Geophys. Res.,* **110,** B10401, doi:10.1029/2005JB003689.

Hodgkinson, K., Stein, R.S. & Marshall, G., 1996. The 1954 Rainbow mountain-Fairview peak-Dixie valley earthquake sequences: a triggered normal faulting sequence, *J. Geophys. Res.,* **101,** 25 459–25 472.

Hurst, K.J. et al., 2000. The coseismic geodetic signature of the 1999 Hector Mine Earthquake, *Geophys. Res. Lett.,* **27,** 2733–2736.

Jackson, D.D., Zheng-kang, S., Potter, D., Ge, X-B & Sung, L-y, 1997. Southern California Deformation, *Science,* **277,** 1621–1622.

Jacoby, G.C. Jr., Shepard, P.R. & Sieh, K.E., 1988. Irregular recurrence of large earthquakes along the San Andreas fault in southern California—evidence from trees near Wrightwood, *Science,* **241,** 196–199.

Jaeger, J. & Cook, N., 1979. *Fundamentals of Rock Mechanics,* 3rd ed., Chapman and Hall, London.

Johnson, K.M. & Segall, P., 2004. Viscoelastic earthquake cycle models with deep stress-driven creep along the San Andreas fault system, *J. Geophys. Res.,* **110,** B05S14, doi:10.1029/2004JB003096.

Kagan, Y.Y., Jackson, D.D. & Liu, Z., 2005. Stress and earthquakes in southern California, 1850–2004, *J. Geophys. Res.,* **110,** B05S14, doi:10.1029/2004JB003313.

Kagan, Y.Y., Jackson, D.D. & Rong, Y.F., 2006. A new catalog of southern California earthquakes, 1800–2005, *Seismological Res. Lett.,* **77**(1), 30–38.

Kenner, S.J. & Segall, P., 2003. Lower crustal structure in northern California: implications from strain rate variations following the 1906 San Francisco earthquake, *J. Geophys. Res.,* **108,** 10.1029/2001JB000189.

Kenner, S.J. & Simons, M., 2005. Temporal clustering of major earthquakes along individual faults due to post-seismic reloading, *Geophys. J. Inter.,* **160,** 179–194.

Kilb D., Gomberg, J. & Bodin, P., 2000. Triggering of earthquake aftershocks by dynamic stresses, *Nature,* **408,** 570–574.

King, G.C.P. & Cocco, M., 2001. Fault interactions by elastic stress changes: new clues from earthquake sequences, *Adv. Geophys.,* **44,** 1–38.

King, G.C.P., Stein, R.S. & Lin, J., 1994. Static stress changes and triggering of earthquakes, *Bull. Seism. Soc. Am.,* **84,** 935–953.

Lin, J. & Stein, R.S., 2004. Stress triggering in thrust and subduction earthquakes and stress interaction between the southern San Andreas and nearby thrust and strike-slip faults, *J. Geophys. Res.,* **109,** doi:10.1029/2003JB002607.

Marsan, D. & Bean, C.J., 2003. Seismicity response to stress perturbations, analyzed for a world-wide catalogue, *Geophys. J. Inter.,* **154,** 179–195.

Meade, B.J. & Hager, B.H., 2005. Block models of crustal motion in southern California constrained by GPS measurements, *J. Geophys. Res.,* **110,** doi:10.1029/2004JB003209.

Nalbant, S., Hubert, A. & King, G.C.P., 1998. Stress coupling between earthquakes in northwest Turkey and the north Aegean sea, *J. Geophys. Res.,* **103,** 24469–24486.

Nostro, C., Cocco, M. & Belardinelli, M., 1997. Static stress changes in extensional regimes: an application to southern Apennines (Italy), *Bull. Seism. Soc. Am.,* **87,** 234–248.

Parsons, T., 2002. Post-1906 stress recovery of the San Andreas fault system calculated from three-dimensional finite element analysis, *J. Geophys. Res.,* **107,** doi:10.1029/2001JB001051.

Parsons, T., 2006. Tectonic stressing California modeled from GPS observations, *J. Geophys. Res.,* **111,** doi:10.1029/2005JB003946.

Parsons, T., Stein, R.S., Simpson, R. & Reasenberg, P., 1999. Stress sensitivity of fault seismicity: a comparison between limited-offset oblique and major strike-slip faults, *J. Geophys. Res.,* **104,** 20183–202.

Parsons, T., Toda, S., Stein, R.S., Barka, A. & Dietrich, J.H., 2000. Heightened odds of large earthquakes near Istanbul: an interaction-based probability calculation, *Science,* **288,** 661–665.

Pollitz, F.F., 1995. Consequences of stress changes following the 1891 Nobi earthquake, Japan. *Bull. Seism. Soc. Am.,* **85,** 796–807.

Pollitz, F.F., 1996. Coseismic deformation from earthquake faulting on a layered spherical earth, *Geophys. J. Int.,* **125,** 1–14.

Pollitz, F.F., 1997. Gravitational-viscoelastic postseismic relaxation on a layered spherical earth. *J. Geophys. Res.,* **102,** 17 921–17 941.

Pollitz, F.F., 2003. Transient rheology of the uppermost mantle beneath the Mojave Desert, California, *Earth Planet. Sci. Lett.,* **215,** 89–104.

Pollitz, F.F. & Nyst, M., 2005. A physical model for strain accumulation in the San Francisco Bay Region, *Geophys. J. Int.,* **160,** 302–317.

Pollitz, F.F. & Sacks, I.S., 1992. Modeling of postseismic relaxation following the great 1857 earthquake, southern California, *Bull. Seism. Soc. Am.,* **82,** 454–480.

Pollitz, F.F. & Sacks, I.S., 2002. Stress triggering of the 1999 Hector Mine earthquake by transient deformation following the 1992 Landers earthquake, *Bull. Seism. Soc. Am.,* **87,** 1–10.

Pollitz, F.F., Peltzer, G. & Bürgmann, R., 2000. Mobility of continental mantle; Evidence from postseismic geodetic observations following the 1992 Landers earthquake, *J. Geophys. Res.,* **105,** 8035–8054.

Pollitz, F.F., Vergnolle, M., & Calais, E., 2003. Fault interaction and stress triggering of 20th century earthquakes in Mongolia, *J. Geophys. Res.,* **108,** doi:10.1029/2002JB002375.

Reasenberg, P. & Simpson, R., 1992. Response of regional seismicity to the static stress change produced by the Loma Prieta earthquake, *Science,* **255,** 1687–1690.

Rockwell, T.K., Lindvall, S., Herzberg, M., Murbach, D., Dawson, T. & Berger, G., 2000. Paleoseismology of the Johnson Valley, Kickapoo, and Homestead Valley faults: Clustering of earthquakes in the eastern California shear zone, *Bull. Seismol. Soc. Am.,* **90,** 1200–1236.

Rydelek, P. & Sacks, I., 2001. Migration of large earthquakes along the san Jacinto fault; stress diffusion from the 1857 Fort Tejon earthquake, *Geophys. Res. Lett.,* **28,** 3079–3082.

Savage, J.C. & Lisowski, M., 1998. Viscoelastic coupling model of the San Andreas fault along the Big Bend, southern California, *J. Geophys. Res.,* **103,** 7281–7292.

Scholz, C.H. , 2002. *The Mechanics of Earthquakes and Faulting,* 2nd ed., Cambridge Univ. Press, New York.

Scholz, C.H., 1988. Mechanics of seismic quiescences, *Pure Appl. Geophys.,* **126,** 701–718.

Segall, P., 2002. Integrating geologic and geodetic estimates of slip rate on the San Andreas fault system, *Inter. Geo. Rev.,* **44,** 62–82.

Shearer, P.M., 1997. Improving local earthquake locations using the L1 norm and waveform cross correlation: application to the Whittier Narrows, California, aftershock sequence, *J. Geophys. Res.,* **102,** 8269–8283.

Shen, Z.-K. *et al.*, 2003. Southern California Earthquake Center Crustal Motion Map Version 3.0, http://epicenter.usc.edu/cmm3/, University of Southern California, Los Angeles, California.

Shewchuk, J.R., 1996, Triangle: Engineering a 2D Quality Mesh Generator and Delaunay Triangulator, First Workshop on Applied Computational Geometry (Philadelphia, PA), 124–133.

Sieh, K.E., Stuiver, M. & Brillinger, D., 1989. A more precise chronology of earthquakes produced by the San Andreas fault in southern California, *J. Geophys. Res.,* **94,** 603–623.

Smith, B.R. & Sandwell, D.T., 2003. Coulomb stress accumulation along the San Andreas Fault system, *J. Geophys. Res.,* **108**(B6), 2296, doi:10.1029/2002JB002136.

Smith, B.R. & Sandwell, D.T., 2006. A model of the earthquake cycle along the San Andreas Fault system for the past 1000 years, *J. Geophys. Res.,* **111,** doi:10.1029/2005JB003703.

Stein, R.S. & Ekström, G.E., 1992. Seismicity and geometry of a 110-km long blind thrust fault, 2, Synthesis of the 1982–85 California earthquake sequence, *J. geophys. Res.,* **97,** 4865–4883.

Stein, R.S. & Lisowski, M., 1983. The 1979 Homestead Valley earthquake sequence, California: control of aftershocks and postseismic deformation, *J. Geophys. Res.,* **88,** 6477–6490.

Stein, R.S., King, G.C.P. & Lin, J., 1992. Change in failure stress on the southern San Andreas fault system caused by the 1992 magnitude = 7.4 Landers earthquake, *Science,* **258,** 1328–1332.

Stein, R., King, G. & Lin, J., 1994. Stress triggering of the 1994 M_w = 6.7 Northridge, California earthquake by its predecessors, *Science,* **265,** 1432–1435.

Stein, R.S., 1999. The role of stress transfer in earthquake occurrence. *Nature,* **402,** 605–609.

Stein, R.S., 2003. Earthquake conversations, *Sci. Amer.,* **288,** 72–79.

Thatcher, W., 1983. Nonlinear strain buildup and the earthquake cycle on the San Andreas fault, *J. Geophys. Res.,* **88,** 5893–5902.

Toda, S., Stein, R.S., Reasonberg, P., Dieterich, J. & Yoshida, A., 1998. Stress transferred by the 1995 Mw = 6.9 Kobe, Japan, shock: effect on aftershocks and future earthquake probabilities, *J. Geophys. Res.,* **103,** 24 543–24 565.

Toda, S. & Stein, R.S., 2002. Response of the San Andreas fault to the 1983 Coalinga-Nuñez earthquakes: an application of interaction-based probabilities for Parkfield, *J. Geophys. Res.,* **107**(B6), 2126, doi:10.1029/2001JB000172.

Toda, S. & Stein, R., 2003. Toggling of seismicity by the 1997 Kagoshima earthquake couplet: a demonstration of time-dependent stress transfer, *J. Geophys. Res.,* **108**(B12), 2567, doi:10.1029/2003JB002527.

Toda, S., Stein, R.S., Richards-Dinger, K. & Bozkurt, S.B., 2005. Forecasting the evolution of seismicity in southern California: animations built on earthquake stress transfer, *J. Geophys. Res.,* **110,** B05S16, doi:10.1029/2004JB003415.

Turcotte, D.L. & Schubert, G., 2002. *Geodynamics,* 2nd edn, Cambridge University Press, pp. 456.

Wdowinski, S., Sudman, Y. & Bock, Y., 2001. Geodetic detection of active faults in southern California, *Geophys. Res. Lett.,* **28,** 2321–2324.

Wyss, M. & Wiemer, S., 2000. Change in the probability for earthquakes in southern California due to the Landers magnitude 7.3 earthquake, *Science,* **290,** 1334–1338.

Zeng, Y., 2001. Viscoelastic stress-triggering of the 1999 Hector Mine earthquake by the 1992 Landers earthquake, *Geophys. Res. Lett.,* **28,** 307–3010.

Zoback, M.D. *et al.* 1987. New evidence on the state of stress of the San Andreas fault system, *Science,* **238,** 1105–1111.

SUPPLEMENTARY MATERIAL

The following supplementary material is available for this article:

Appendix S1. Containing supplementary Figs S1 to S6.

This material is available as part of the online article from:
http://www.blackwell-synergy.com/doi/abs/10.1111/j.1365-246X.2007.03391.x
(This link will take you to the article abstract).

Please note: Blackwell Publishing are not responsible for the content or functionality of any supplementary materials supplied by the authors. Any queries (other than missing material) should be directed to the corresponding author for the article.